COMPUTER RESEARCH AND MODELING
2022 VOL. 14 NO. 1 P. 115–126
DOI: 10.20537/2076-7633-2022-14-1-115-126

КиМ

MODELS IN PHYSICS AND TECHNOLOGY

UDC: 355.469.34:004.94

The dynamic model of a high-rise firefighting drone

N. D. Anh[1], P. H. Hai[1], N. T. H. Hanh[1], N. Q. Vinh[2,3,a]

[1]The University of Fire prevention and Fighting,
234, Khuat Quy Tien, Thanh Xuan, Ha Noi, Viet Nam
[2]Automatic Control System Department, Bauman Moscow State Technical University,
5, 2-d Baumanskaya st., Moscow, 107005, Russia
[3]Department of Automatic control, Academy of Military Science and Technology,
17, Hoang Sam, Cau Giay, Ha Noi, Viet Nam

E-mail: [a] vinhquang2808@mail.ru

Received 29.10.2021, after completion — 19.01.2022.
Accepted for publication 08.02.2022.

The utilization of unmanned aerial vehicles (UAVs) in high-rise firefighting operations is the right solution for reaching the fire scene on high floors quickly and effectively. The article proposes a quadrotor-type firefighting UAV model carrying a launcher to launch a missile containing fire extinguishing powders into a fire. The kinematic model describing the flight kinematics of this UAV model is built based on the Newton – Euler method when the device is in normal motion and at the time of launching a firefighting missile. The results from the simulation testing the validity of the kinematic model and the simulation of the motion of the UAV show that the variation of Euler angles, flight angles, and aerodynamic angles during a flight are within an acceptable range and overload guarantee in flight. The UAV flew to the correct position to launch the required fire-extinguishing ammunition. The results of the research are the basis for building a control system of high-rise firefighting drones in Vietnam.

Keywords: firefighting, aerospace control, dynamical, simulation

Citation: *Computer Research and Modeling*, 2022, vol. 14, no. 1, pp. 115–126.

Introduction

Fighting high-rise fires always poses a variety of challenges and difficulties for fire service in the world due to the limited accessibility of fire apparatuses to fire and explosion locations on high floors. The fire in an office building in Dhaka, the capital of Bangladesh on March 28, 2019, which killed 19 people, or the Grenfell tower fire in London, England on June 14, 2017, which killed 70 people are obvious examples of these difficulties, etc. In Vietnam and some developing countries, the density of commercial centers and high-rise buildings is high due to rapid urbanization and limited land fund, thus narrowing the distance between buildings. The narrow space in urban areas causes difficulties in the access and organization of firefighting operations [Himoto et al., 2008].

Researchers from around the world have proposed a number of models of UAVs for firefighting. These models are mainly built in two groups to employ two methods of discharging firefighting agents into a fire [Radu et al., 2019] as follows.

Group 1: Firefighting UAV model with the payload drop mechanism. The research [Aydin et al., 2019] proposes the use of a model of quadrotor-type UAS (unmanned aircraft system) carrying a fire extinguishing ball dropped from above to fight forest fires, outdoor bushes, etc. Firefighting balls which are designed with a mass of 1,3–1,5 kg are capable of fighting fires effectively within a radius of up to 1,3 m. Each UAS is designed with a payload of 15 kg (equivalent to about 10 fire extinguishing balls) and with a calculated firefighting area of 676 m^2. In the study [Aydin et al., 2019], the author proposes a quadrotor-type UAV model which carries and releases a firefighting ball with the mechanism of two mechanical claws. The fire extinguishing ball contains Monoammonium Phosphate as the fire extinguishing agent and is made of a lightweight mixture: gypsum and rubber based bonding agent. When being tested practically, the effectiveness of firefighting of each UAV firefighting ball is from 1,8 to 2 m^2. The research [Alshbatat, 2018] proposes a firefighting quadrotor model which is capable of releasing up to 4 fire extinguishing balls at the same time with a servo motor. This payload drop mechanism shows smaller horizontal area for fitting most of the drones as well as less effect of vibrations during flight. Firefighting balls are proposed in the study [Soliman, Cagan, Buldum, 2019]. The advantages of the group of the firefighting UAV model with the payload drop mechanism are that the device is of a small size, simple structure, low cost, so it is easy to equip the local fire force. However, the disadvantage of this device is that it is only suitable for fighting outdoor fires (forest fires), difficult to deploy and ineffective for high-rise fires.

Group 2: Firefighting UAV model with the mechanism of propelling fire extinguishing agents forcibly. Aerones company in Latvian designed a 28-propeller firefighting UAV model [Aerones, 2021] in which fire extinguishing agent is water or foam. The device carries a fire hose assembly and a nozzle on the body of the device. Water or foam is pushed from the pump system located on the fire truck at the ground through the hose system, and is directed by the rotation angle of the UAV. The maximum reachable height of the device is 85 m with a flow rate of 98 liters per minute. The advantage of the group of the device using a nozzle to spray fire extinguishing agents on a fire is the ability to fight fires continuously for a long time with the supply (extinguishing agents) from the ground. At the same time, the device easily accesses and fights various types of fires such as high-rise fires, forest fires or fires in areas of complex terrain, etc. However, pulling the fire hoses from the ground to the firefighting position under the impact from the pressure of the pump system on the hoses makes the kinematic model of this type of device relatively complicated. The device must be of a large size, stable mechanical structure and be arranged with numerous propulsion engines which increases its cost. In addition, the device is also limited in the scope of firefighting by the covering and separating structures of the building.

Based on the above advantages and disadvantages, with the goal of approaching and fighting high-rise fires, the researchers propose the model of the proposed high-rise firefighting drone which

has a quadrotor configuration carrying a camera and a firefighting rocket launcher figure 1 has the following characteristics [Vinh, 2017].

- Quadrotor frame with 4 symmetrically arranged X-shaped propellers plays the role of generating thrust and balance, allowing the device to have the ability to take off and land vertically. The entire movement of the device is controlled by changing the engine speed, so compared to other types of UAVs, the quadrotor has a simpler mechanical structure. In addition, because of the axial symmetry, the inertia effects will be reduced, resulting in a simpler controller. Its simple structure and small size allow the fire service to transport the equipment easily. The ability to take off on the spot enables the quadrotor to operate in urban areas which are narrow and full of obstacles.
- In the middle of the device frame structure there is a control center, of which the shell is made of non-combustible material and is of low specific gravity.
- A firefighting rocket launcher is located below the control center. Its operation activates propellants creating thrust to launch the rocket carrying the extinguishing agents into the fire. The structure of the firefighting rocket is designed to ensure the ability to penetrate the glass doors and windows of the room. This allows the proposed device to be able to extinguish the fire from a distance and keep a safe distance from the fire.
- The camera is installed on the device with the task of collecting images from the fire and acting as a viewfinder to identify the location to launch the firefighting rocket.
- The drone is remotely controlled by firefighters via radio waves at the control station located near the fire location.

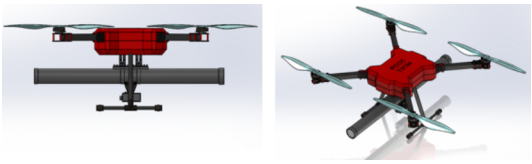

Fig. 1. Proposed firefighting quadrotor Model

The kinematic model of the high-rise firefighting drone

The kinematic model of the high-rise firefighting drone is built according to the Newton – Euler method with the following assumptions [Vinh et al., 2020]:

- ignoring the elastic deformation factors due to the device frame structure, considering the device as an absolute solid with symmetrical structure;
- the device propellers are solid, so aerodynamic effects due to the blade flapping effect are eliminated;
- ignoring ground effect.

These factors will have a relatively small or short-lived impact on the total device up time. We can therefore ignore these effects to simplify the equations of motion. This method has been proven effective in practice through previous study [Bouabdallah, 2007]. Considering the frame structure an

absolute solid ignores the kinematic effects of mechanical joints, the elasticity of the frame structure, and the propellers, allowing the problem to be solved in terms of analyzing an absolute solid with 6 degrees of freedom. Considering the device symmetric allows ignoring the components of the moment of inertia.

Frame and coordinate system transformation matrix

To describe the movements of the device, the following two reference frames are used [Luukkonen, 2011].

- Inertial reference frame E: is a frame of reference without acceleration, in which Newton's laws are satisfied. The coordinate system associated with this frame has the origin of coordinates (symbolized by OE) attached to an object that is fixed relative to Earth. The position of the center of gravity of the drone in the inertial coordinate system and is represented by a vector $\xi^E = (x, y, z)$. The vector $\Theta^E = (\phi, \theta, \psi)$ describes the direction of the device. The vector describes the direction of the device. The vector Φ is used to describe the position and orientation of the device in the inertial coordinate system: $\Phi = [\xi^E \Theta^E]^T$.
- Reference system attached to the drone [Chen et al., 2016]: is a fixed frame of reference which moves along with the drone. The origin O^B of the coordinate system attached to the object is taken to coincide with the center of gravity of the device. The coordinate axes are denoted by x^B, y^B, z^B. The vector $v^B = [u\ v\ w]^T$ and $\omega^B = [p\ q\ r]^T$ describe the linear and angular velocity vectors of the device, respectively. The dimensional convention of reference systems is as shown in figure 2.

Rotation matrix ${}^E_B R(\phi, \theta, \psi)$ converts from object-mounted coordinate system to inertial coordinate system:

$$ {}^E_B R(\phi, \theta, \psi) = R_Z(\psi) R_Y(\theta) R_X(\phi) = G_{3x3}, \tag{1} $$

inside $G_{11} = c(\theta)c(\psi)$, $G_{12} = s(\phi)s(\theta)c(\psi) - c(\phi)s(\psi)$, $G_{13} = c(\phi)s(\theta)c(\psi) + s(\phi)s(\psi)$, $G_{21} = c(\theta)s(\psi)$, $G_{22} = s(\phi)s(\theta)s(\psi) + c(\psi)c(\phi)$, $G_{23} = c(\phi)s(\theta)s(\psi) - s(\phi)c(\psi)$, $G_{31} = -s(\theta)$, $G_{32} = s(\phi)c(\theta)$, $G_{33} = c(\phi)c(\theta)$. Here, $c = \cos$, $s = \sin$. Note: the coordinate transformation matrix is orthogonal, so ${}^E_B R^{-1} = {}^B_E R = {}^E_B R^T$.

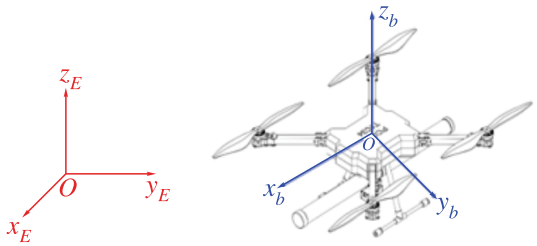

Fig. 2. Inertial reference frame and reference system attached to the drone

Description of device movement

The drone is designed with two pairs of reversible propellers, of which two propellers rotating on the same side are arranged opposite each other. By adjusting the speeds of these four propellers reasonably, the drone will make the movements and navigation as required. The thrust of propellers [Bouabdallah, 2007; Sabatino, 2015]:

$$ F_i = c_t \omega_i^2. \tag{2} $$

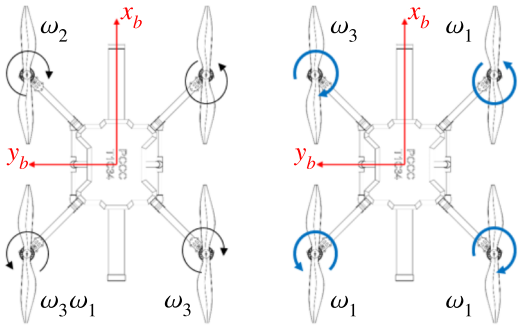

a) Supension b) Height rise

Fig. 3. Movements of the device along the z-axis

Here, c_t is the thrust coefficient of the propellers ($\mathrm{N} \cdot \mathrm{s}^2$) and ω_i is the angular velocity of the i_{th} propeller (rad/s). The movement in space of the device is divided into the following motion.

Suspension motion (keeping balance at a certain height) or height rise/fall

To perform suspension motion, the vehicle must control the propellers to rotate at the same speed to create a thrust balanced with gravity, and at the same time suppresses the moments causing rotation. Increasing or decreasing the rotational speed creates height-based up and down movements. Note that the propellers must rotate at the same speed, so that the torque generated by four propellers cancels each other out, thus keeping the direction of the vehicle unchanged. The combined thrust generated by the four propellers on the device-mounted frame of reference:

$$U_1 = c_t(\omega_1^2 + \omega_2^2 + \omega_3^2 + \omega_4^2). \tag{3}$$

Roll motion (rotation around the Ox_b axis)

To perform Roll rotation around the Ox_b axis, it is necessary to adjust the speeds of the propellers 2 and 4 while the velocities of propellers 1 and 3 remain constant. If the speed propeller 2 (left) is higher than that of propeller 4 (right), the device will rotate in a clockwise direction around the X_b axis, otherwise, it reverses the rotation. This rotation occurs because of the moment difference between two sides of the propellers of the device. Formula (4) represents the value of the total moment on the reference frame mounted on the device:

$$U_2 = c_t \times l \times \cos(45)(-\omega_1^2 + \omega_2^2 + \omega_3^2 - \omega_4^2). \tag{4}$$

Along with the rotation, the device will move accordingly. The device moves forward with a right rotation figure 3 and backward with a left rotation around the Y_b axis.

Pitch motion (rotation around the Oy_b axis)

To perform a Pitch rotation around the Oy_b axis, it is necessary to adjust the speeds of propellers 1 and 3 while the velocities of propellers 2 and 4 are kept constant. If the speed of propeller 1 (front) is higher than that of propeller 3 (rear), the device will rotate right around the Oy_b axis, otherwise, it will rotate left. This rotation occurs because of the moment difference between the two sides of the propellers of the device. Equation (5) represents the value of the moment on the reference frame mounted on the device:

$$U_3 = c_t \times l \times \cos(45)(-\omega_1^2 - \omega_2^2 + \omega_3^2 + \omega_4^2). \tag{5}$$

Along with the rotation, the device will move accordingly. The device moves forward with a right rotation (Figure 3) and backward with a left rotation around the Oy_b axis.

Yaw motion (rotation around the Oz_b axis)

To make Yaw motion clockwise on the Oz_b axis, it is necessary to adjust the speeds of the propellers 2, 4 to increase by $\Delta\omega$, and the speeds of the propellers 1, 3 to decrease by $\Delta\omega$. Increasing and decreasing by the same amount ensures the same height of the device when making Yaw movement. To make Yaw movement counter-clockwise on the Oz_b axis, it is necessary to adjust the speeds of the propellers 2, 4 to decrease by a and the speeds of the propellers 1, 3 to increase by $\Delta\omega$. Formula (6) describes the relationship between the total torque around the Yaw axis with the speeds of the four propellers on the frame of reference attached to the object, where C_q is the coefficient of the ratio of the moment to the rotational velocity.

$$U_4 = c_q(-\omega_1^2 + \omega_2^2 - \omega_3^2 + \omega_4^2). \tag{6}$$

From (3) to (6) the force and torque generated from the rotational speed of the propellers are summed up as follows:

$$\begin{cases} U_1 = c_t(\omega_1^2 + \omega_2^2 + \omega_3^2 + \omega_4^2), \\ U_2 = c_t \cdot l \cdot \cos(45)(-\omega_1^2 + \omega_2^2 + \omega_3^2 - \omega_4^2), \\ U_3 = c_t \cdot l \cdot \cos(45)(-\omega_1^2 - \omega_2^2 + \omega_3^2 + \omega_4^2), \\ U_4 = c_q(-\omega_1^2 + \omega_2^2 - \omega_3^2 + \omega_4^2). \end{cases} \tag{7}$$

Kinematic model

The kinematic model describes the motion of the device in reference frames through velocity equations, thereby determining the position and orientation of the object [Kurak, Hodzic, 2018; Sabatino, 2015].

Linear Velocity

The relationship between the linear velocity of the device in the inertial frame of reference and the reference frame on the body is as follows:

$$\dot{\xi}^E = {}^E_B R(\phi, \psi, \theta) \times v^B. \tag{8}$$

Angular velocity

The matrix converting from the angular velocity $\dot{\Theta}^E = (\dot{\phi}, \dot{\theta}, \dot{\psi})$ in the inertial reference frame to the angular velocity $\omega^B = (pqr)$ in the reference frame on the object is as follows [Himoto et al., 2008]:

$$\omega^B = {}^B_E T \dot{\Theta}^E, \tag{9}$$

$${}^B_E T = \begin{bmatrix} 1 & 0 & -s(\theta) \\ 0 & c(\phi) & s(\phi)c(\theta) \\ 0 & -s(\phi) & c(\phi)c(\theta) \end{bmatrix}. \tag{10}$$

From (8) to (10) the kinematic model of the device is as follows [Aydin et al., 2019]:

$$F^B = [F_x^B F_y^B F_z^B]^T. \tag{11}$$

The dynamic model of the high-rise firefighting drone

Force balance equation

Let $F^B = [F_x^B F_y^B F_z^B]^T$ be the analytical net force along the coordinate axes of the reference frame mounted on the object. In an inertial frame of reference, applying Newton's 2nd law we have [Chen et al., 2016; Li, Wang, Gai, 2011; Stevens, Lewis, Johnson, 2015]:

$$m\frac{d^2\xi^E}{dt^2} = {}_B^E R \times F^B \Leftrightarrow m\frac{d\left({}_B^E R \cdot v^B\right)}{dt} = {}_E^B R \cdot F^B. \tag{12}$$

In space the combined force acting F^B on the device includes Gravity and thrust of 4 propellers. Therefore, on the body-mounted frame of reference:

$$\begin{bmatrix} F_x^B \\ F_y^B \\ F_z^B \end{bmatrix} = \begin{bmatrix} mg[s(\theta)] \\ -mg[s(\phi)c(\theta)] \\ -mg[c(\phi)c(\theta)] + U_1 \end{bmatrix}. \tag{13}$$

Replacing (13) into (8) we have:

$$\begin{cases} \ddot{x} = \dfrac{U_1}{m}[s(\phi)s(\psi) + c(\phi)c(\psi)s(\theta)], \\ \ddot{y} = \dfrac{U_1}{m}[c(\phi)s(\psi)s(\theta) - c(\psi)s(\phi)], \\ \ddot{z} = -g + \dfrac{U_1}{m}[c(\phi)c(\theta)]. \end{cases} \tag{14}$$

The equilibrium equation of moment

Applying the Newton – Euler method to the rotation of the device in the frame of reference mounted on the object, we have the following equation [Zhu et al., 2015]:

$$M_B = I_r\dot{\omega}^B + \omega^B \times I_r\omega^B + M_G. \tag{15}$$

Inside

$$I_r = \begin{bmatrix} I_{xx} & 0 & 0 \\ 0 & I_{yy} & 0 \\ 0 & 0 & I_{zz} \end{bmatrix}. \tag{16}$$

I_{xx}, I_{yy}, I_{zz} ($\text{kg} \cdot \text{m}^2$) are the moments of inertia along the Ox_b, Oy_b, Oz_b axes of the UAV.

From (15) we have

$$I\dot{\omega} = M_B - \omega^B \times I\omega^B - M_G; \tag{17}$$

$$\begin{cases} \dot{p} = \dfrac{I_{yy} - I_{zz}}{I_{xx}}qr + \dfrac{J_r\omega_r}{I_{xx}}q + \dfrac{U_2}{I_{xx}}, \\ \dot{q} = \dfrac{I_{zz} - I_{xx}}{I_{yy}}qr - \dfrac{J_r\omega_r}{I_{yy}}p + \dfrac{U_3}{I_{yy}}, \\ \dot{r} = \dfrac{I_{xx} - I_{yy}}{I_{zz}}pq + \dfrac{U_4}{I_{zz}}. \end{cases} \tag{18}$$

Changes in specifications of the device when launching firefighting rockets

At the time of launching the firefighting rocket, two changes are affecting the aerodynamic model of the drone: the first is the change in center of gravity, weight, and moment of inertia, the second is the reaction force of the rocket which impacting on the drone [Sagy, Braun-Lewensohn, 2009].

The change of center of gravity and weight of the device when launching the rocket

After launching a firefighting rocket:

– the weight of the drone changes as follows: $m_s = m - m_{rocket}$; m_{rocket} is the mass of the firefighting rocket (kg); m is the mass of the UAV before launching the rocket (kg); m_s is the mass of the UAV after launching the rocket (kg);

– the position of the center of gravity of the UAV changes as follows:

$$\Delta i_b = \frac{m_{rocket} i_{rocket}}{m_s} \quad (i = x, y, z); \tag{19}$$

$\{x_{rocket}, y_{rocket}, z_{rocket}\} = \{0, 0, z_{rocket}\}$ is the focus coordinates of the rocket relative to the center of gravity of the UAV before launching the rocket; firefighting rockets are arranged symmetrically through the planes $O_bX_bZ_b$ and $O_bY_bZ_b$, so after launching the rocket, the focus coordinates of the drone only change in height compared to the former center of gravity;

– the moment of inertia changes as follows:

$$I_s = \begin{bmatrix} I_{sxx} & 0 & 0 \\ 0 & I_{syy} & 0 \\ 0 & 0 & I_{szz} \end{bmatrix}. \tag{20}$$

I_{sxx}, I_{syy}, I_{szz} (kg·m^2) are the moments of inertia along the X_b, Y_b, Z_b axes after the UAV launches the firefighting rocket.

Reaction force during the launch of firefighting rockets

The structure of the firefighting rocket system consists of two main components: the launch tube and the firefighting rocket. The launch tube is an alloy tube that is one meter long, open at both ends, and equipped with a triggering device to create sparks to launch firefighting rockets. Firefighting rockets include warheads, fire extinguishing agents, and propellants. The warhead is used for flight navigation and penetration increase; the fire extinguishing agent which is inside the rocket activates itself when reaching the fire; an amount of propellant is placed at the end of the rocket as shown in figure 4. When activated, the propellant will push the rocket out of the launch tube (the thrust F_{thrust}) and ignite a flow of combustible gases behind the launch tube (Reaction force $F_{reaction}$). According to Newton's 2nd law: $F_{thrust} \approx -F_{reaction}$. Two forces that are of equal value but in the opposite directions help to suppress the forces affected during the launch of the firefighting rocket to the drone. However, when the rocket moves inside the launch tube, it will generate frictional force F_{ms} acting on the drone. This force is generated in a very short time, approximately ms, with a limited amplitude (depending on the coefficient of friction between two contacting surfaces and the magnitude of the pressure). Therefore, the force acting on the drone when launching a firefighting rocket tends to push the drone backward in the direction $\overrightarrow{Ox_b}$ and has a value equal to

$$F_{action} = \begin{cases} -F_{ms} \ (0 < t < \tau), \\ 0 \ (t > \tau). \end{cases}$$

Where F_{ms} is the frictional force during the rocket's movement in the launch tube (N). τ is the travel time of the rocket in the launch tube (s).

This force also causes the Pitch angular rotation moment:

$$M_{action} = \begin{cases} M_{ms} \ (0 < t < \tau), \\ 0 \ (t > \tau). \end{cases} \tag{21}$$

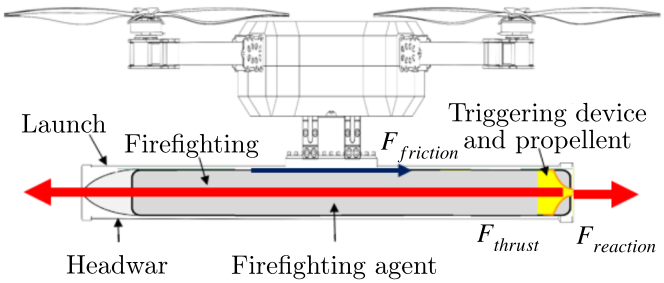

Fig. 4. Forces acting on the drone during the process of launching the firefighting rocket

Where: M_{ms} is the moment created by F_m acting on the drone caused during the launch of the firefighting rocket (N).

Combined (18), the kinematic model of the device during the launch of the firefighting rocket is as follows:

$$\begin{cases} \dot{p} = \dfrac{I_{yy} - I_{zz}}{I_{xx}} qr + \dfrac{J_r \omega_r}{I_{xx}} q + \dfrac{U_2}{I_{xx}}, \\ \dot{q} = \dfrac{I_{zz} - I_{xx}}{I_{yy}} qr - \dfrac{J_r \omega_r}{I_{yy}} p + \dfrac{U_3}{I_{yy}} + M_{ms}, \\ \dot{r} = \dfrac{I_{xx} - I_{yy}}{I_{zz}} pq + \dfrac{U_4}{I_{zz}}; \end{cases} \tag{22}$$

$$\begin{cases} \dot{u} = gs(\theta) - qw + rv - \dfrac{F_{ms}}{m}, \\ \dot{v} = -g[s(\phi)c(\theta)] - ru + pw, \\ \dot{w} = -g[c(\phi)c(\theta)] + \dfrac{U_1}{m} - pv + qu. \end{cases} \tag{23}$$

Table 1. Physical parameters of the built quadrotor

Parameters	Value	Units
Mass	7,34	kg
Length motor to motor	700	mm
Moment of Inertia I_{xx}	0,161	$kg \cdot m^2$
Moment of Inertia I_{yy}	0,308	$kg \cdot m^2$
Moment of Inertia I_{zz}	0,332	$kg \cdot m^2$
Motor Constant	1089	rpm/V
Coefficient thrust	$1{,}15 \cdot 10^{-3}$	$N \cdot s^2$
Coefficient torque	$1{,}06 \cdot 10^{-7}$	$N \cdot m \cdot s^2$

Simulation and experiment results

This section presents experiments that have been executed to demonstrate the performance of the proposed planning algorithm. We make the assumption that the UAV with the actual physical parameters of the implemented quadrotor, show in table 1 moves close to the target in no wind and fires a flame-retardant projectile. Model simulation on matlab shown in figure 5. The UAV flies with the scenario: fly to coordinates example $(0, 0, 32)$, hang there so that at the end of the gun, aim at the predetermined position and fire the fire bullet about 3 m away. The quadrotor simulator is used to check

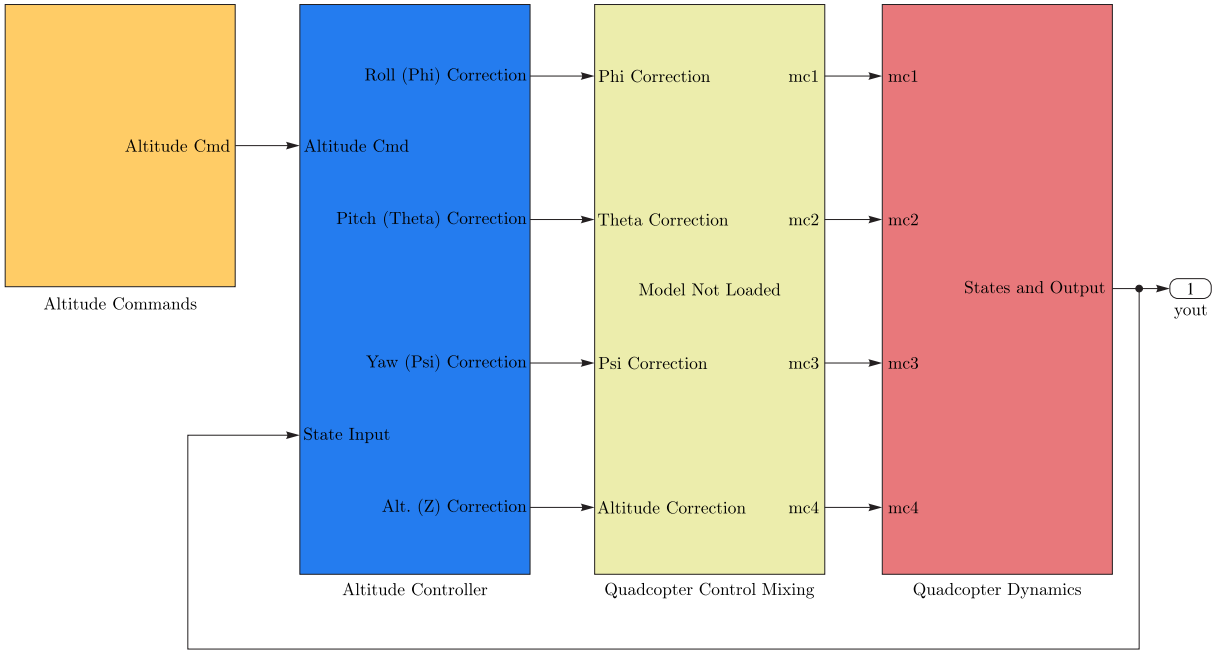

Fig. 5. Model Simulation

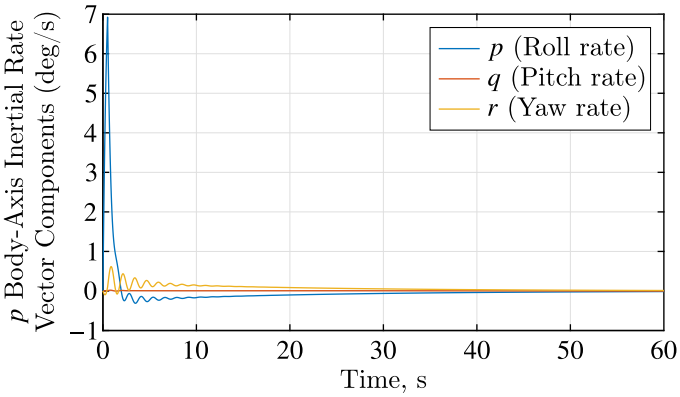

Fig. 6. Yaw, Pitch, Roll Angle

the validity of the kinematic model of the quadrotor and simulate the motion of the UAV. Figure 7 shows the variation of Euler angles φ, θ, ψ and variation of flight angles and aerodynamic angles during flight which are in acceptable range and ensure stable flight characteristics and some parameters obtained for this movement are depicted in figure 6. In figure 8 shows the 3-D flight trajectory plots respectively and figure 9 shows an experimental flight program of a firefighting aircraft.

Conclusion

In this article, the process of building a mathematical model describing the flight dynamics of a high-rise fire-fighting drone is performed. The model is made according to the Newton – Euler method with two states of motion: normal time and fire-fighting rocket launch. The obtained results show that the model is reliable, meeting the requirements set forth for further research. In the next process, we will study and update information about the control system of the high-rise fire fighting drone to evaluate its fire fighting effectiveness and apply it in practice in Vietnam.

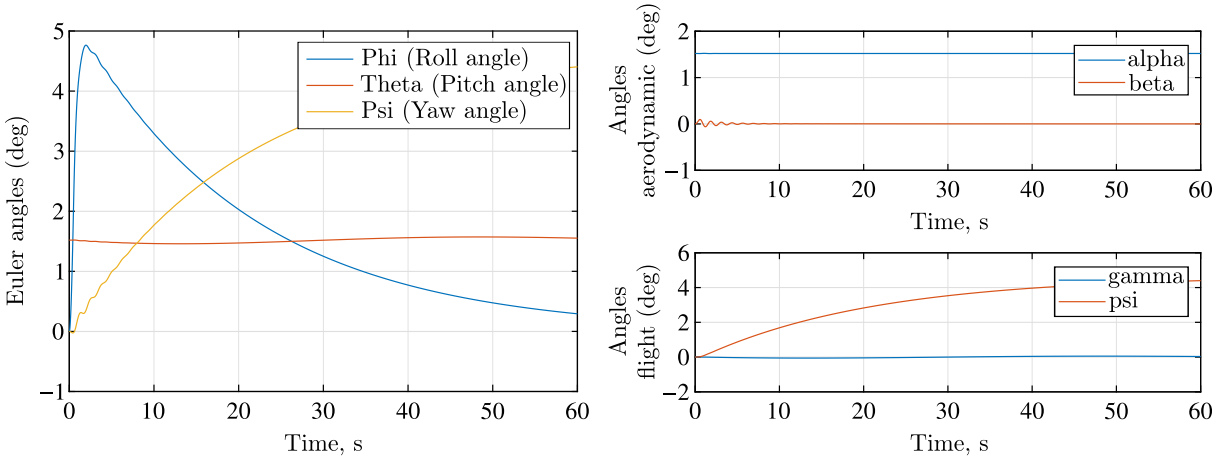

Fig. 7. Variation of Euler angle, flight angles and aerodynamic angles

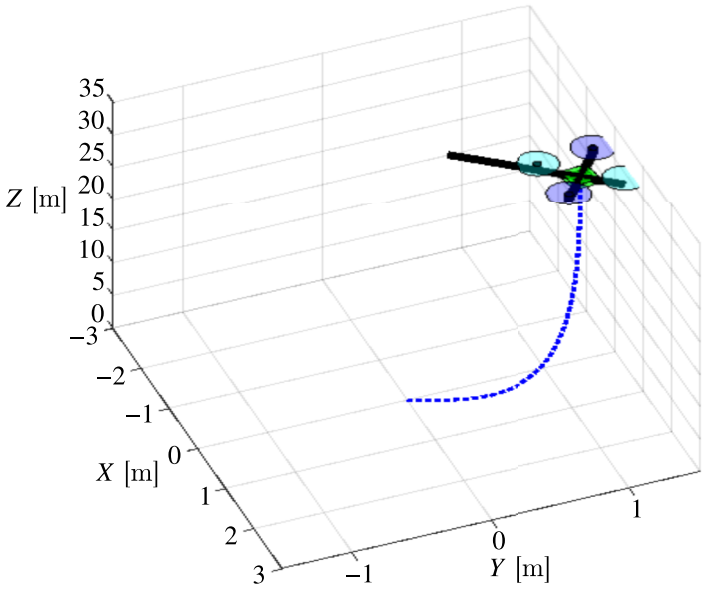

Fig. 8. 3D flight trajectory in Matlab Simmechanic environment

Fig. 9. The designed during flight

References

Aerones DRONE solutions. — 2021. — Retrieved from https://www.aerones.com/other/drone/

Alshbatat A. I. N. Fire extinguishing system for high-rise buildings and rugged mountainous terrains utilizing quadrotor unmanned aerial vehicle // International Journal of Image, Graphics and Signal Processing. — 2018. — Vol. 11. — P. 1–23.

Aydin B., Selvi E., Tao J., Starek M. J. Use of fire-extinguishing balls for a conceptual system of drone-assisted wildfire fighting // Drones. — 2019.

Bouabdallah S. Design and control of quadrotors with application to autonomous flying // Epfl. — 2007.

Chen Y., Yu J., Mei Y., Wang Y., Su X. Modified central force optimization (MCFO) algorithm for 3D UAV path planning // Neurocomputing. — 2016. — Vol. 171. — Pp. 878–888.

Himoto K., Akimoto Y., Hokugo A., Tanaka T. Risk and behavior of fire spread in a densely-built urban area // Fire Safety Science. — 2008. — Vol. 9. — Pp. 267–278.

Kurak S., Hodzic M. Control and estimation of a quadcopter dynamical model // Periodicals Of Engineering And Natural Sciences (PEN). — 2018. — Vol. 6. — P. 63–75.

Li D., Wang H., Gai W. Application of a feedforward controller with a disturbance observer for UAV during missile launch // 2011 2nd International Conference On Artificial Intelligence, Management Science And Electronic Commerce (AIMSEC). — 2011. — Pp. 2811–2815.

Luukkonen T. Modelling and control of quadcopter // Independent Research Project In Applied Mathematics, Espoo. — 2011. — Vol. 22. — P. 22.

Radu V., Tiberiu A., Schmidt K., Saqib M. Use of drones for firefighting operations. — 2019.

Sabatino F. Quadrotor control: modeling, nonlinearcontrol design, and simulation. — 2015.

Sagy S., Braun-Lewensohn O. Adolescents under rocket fire: when are coping resources significant in reducing emotional distress? // Global Health Promotion. — 2009. — Vol. 16. — Pp. 5–15.

Soliman A. M. S., Cagan S. C., Buldum B. B. The design of a rotary-wing unmanned aerial vehicles–payload drop mechanism for fire-fighting services using fire-extinguishing balls // 2019. — Vol. 1. — P. 10.

Stevens B., Lewis F., Johnson E. Aircraft control and simulation: dynamics, controls design, and autonomous systems. — John Wiley Sons, 2015.

Vinh N., Duc Thanh N., Minh Dac H., Dang Khoa T. Identify aerodynamic derivatives of the airplane attitude channel using a spiking neural network // International Journal Of Aviation, Aeronautics, And Aerospace. — 2020. — Vol. 7. — P. 3.

Vinh N. An algorithm for determining the navigation parameters of AUVs based on the combination of measuring devices // Procedia Computer Science. — 2017. — Vol. 103. — Pp. 331–338.

Zhu B., Hou Z., Shan S., Wang X. Equilibrium positions for UAV flight by dynamic soaring // International Journal Of Aerospace Engineering. — 2015. — Vol. 2015.